Available online at www.sciencedirect.com
ScienceDirect
Journal of Sound and Vibration 312 (2008) 801–820
JOURNAL OF SOUND AND VIBRATION
www.elsevier.com/locate/jsvi

A component-based model for aircraft landing gear noise prediction

Yueping Guo*

The Boeing Company, Mail Code H013-B308, 5301 Bolsa Avenue, Huntington Beach, CA 92647, USA

Received 17 May 2006; received in revised form 31 October 2007; accepted 7 November 2007
Available online 21 December 2007

Abstract

This paper follows the general formulation of aircraft landing gear noise prediction to develop a component-based model, incorporating scaling laws of the theory of aerodynamic noise generation and correlations of these scaling laws with currently available test data. The method decomposes the landing gear noise into three spectral components, respectively, for the low, the mid and the high frequencies, which corresponds to cataloging the parts in the landing gear assembly into three groups, namely, the wheels, the main struts, and the small details. For all three spectral components, models are presented for their spectra, far-field directivities and amplitudes. The spectral characteristics of the three components are defined by normalized spectra, as functions of the Strouhal numbers based on the respective length scales of the three groups of parts in the landing gear assembly. Individual directivity factors are also presented for the three spectral components, with the low-frequency component having the smallest variations with emission angle and the high-frequency component having the largest variations. The amplitudes of the three spectral components are correlated to parameters unique to each group of landing gear parts, with the low- and mid-frequency noise essentially characterized by the physical dimensions of the wheels and the main struts, respectively, and the high-frequency noise, whose generation is associated with a large number of small details in practical landing gears, defined by a complexity factor. Quantities that affect this complexity factor are discussed and an empirical model is proposed for practical applications. The prediction model is validated by wing tunnel test data for an isolated Boeing 737 landing gear. In this case, the predictions agree well with data, both in parametric trends and in absolute noise levels.

1. Introduction

Because of the geometric and flow complexity, aircraft landing gear noise prediction has mostly been empirical [1–8]. In most cases, a particular database for a landing gear configuration is used to derive parametric trends and prediction schemes. The empirical approach has certainly proven to be valuable in practical applications. Its limitations and drawbacks, however, are also well recognized, of which the limited parametric range in a particular database and the potential error in the measurements are probably two of the most severe obstacles in empirical modeling. The former limits the validity domain of the empirical prediction,

*Tel.: +1 714 8961527; fax: +1 714 8961559.
E-mail address: yueping.guo@boeing.com

0022-460X/$ - see front matter © 2007 Elsevier Ltd. All rights reserved.
doi:10.1016/j.jsv.2007.11.013

Nomenclature

a	average cross-section dimension of struts
a_j	linear dimension of jth strut cross-section
A	amplitude of normalized spectra
b_j	linear dimension of jth strut cross-section
B	parameter defining normalized spectra
c_0	constant sound speed
d	wheel diameter
d_S	diameter of shock strut
D	directivity factor
EPNL	effective perceived noise level
f	frequency
F	normalized spectrum
h	parameter defining directivity factor
k_0	acoustic wavenumber
ℓ	typical size of small details
ℓ_0	length scale
L	total length of struts
L_j	length of jth strut
M	Mach number of mean flow ahead of landing gear
M_0	flight Mach number
n_i	ith component of surface normal
N	number of wheels
N_s	number of struts
OASPL	overall sound pressure level
p	sound pressure
p_s	surface pressure
R	radial distance of far-field microphone
s_j	perimeter of the jth strut cross-section
S	aggregate surface integration effects
SPL	sound pressure level
St	Strouhal number
t	time
u_0	velocity scale
U	mean flow velocity
w	width of landing gear wheels
W	aircraft takeoff gross weight
$\mathbf{x}$	far-field coordinate vector
$\mathbf{y}$	near-field coordinate vector
α	coefficient of atmospheric absorption
β	radiation efficiency
γ	wheel track alignment angle
Δ	Doppler factor
η	complexity factor
θ	emission angle in flyover plane
μ	controlling high-frequency falloff
Π	far-field noise power spectral density
Π_s	surface pressure power spectral density
ρ_0	constant mean density
σ	power index in normalized spectra
τ	source time
τ_0	time scale
ω	angular frequency
ω_d	Doppler-shifted angular frequency

because of the uncertainties outside the database used to develop the prediction methods, while the latter can lead to wrong or inaccurate parametric trends, if the empirical tools are developed by blunt-force data collapsing without carefully correcting errors in the database. Thus, it is important to advance noise predictions, both by introducing physics-based theory into the modeling so that general scaling laws are utilized to cover a wide range of flow and geometry parameters, and by incorporating a new database into the prediction schemes. This is what has motivated the work reported here; we follow the general formulation of landing gear noise prediction [9] to develop a component-based model for landing gear noise prediction.

We will start with the scaling laws from the theory of aerodynamic noise generation, which identify general trends such as the sixth power law of the Mach number dependence and the inverse fourth power convective amplification [9–14]. This gives the modeling a sound theoretical foundation. The scaling laws will be correlated to available databases [6,7,15–21], as well as recent results from numerical simulations [22–26], so that proportionality constants in the scaling laws will be quantitatively determined and the predictions are not only for the general parametric trends, but also for the absolute noise levels. The scaling laws will be applied to three spectral components of the landing gear noise, namely, the low-, the mid- and the high-frequency noise. The decomposition of landing gear noise into three spectral components has been discussed before [6,7,15]. It results from detailed analyses of landing gear noise test data, which have revealed different characteristics of the measured noise in each individual frequency domains, such as their spectral features, their far-field directivities and their dependencies on the geometric parameters of the gear assembly. The decomposition also reflects the source mechanisms of the noise in different frequency domains; the three groups of landing gear parts, namely, the wheels, the main struts and the small details, such as braces, cutouts, steps, wires, and other small geometry irregularities, have typical sizes that significantly differ from each other. These distinctively

different length scales lead to sound generation of distinctively different characteristic frequencies, supporting the hypothesis that the total landing gear noise is the incoherent summation of the three spectral components.

For all three spectral components, we will model the normalized spectra to define the frequency features, in terms of the Strouhal number based on the flow velocity upstream of the landing gear and the respective length scales of the three groups of landing gear parts. General features of the normalized spectra include the unity maximum at some values of the Strouhal number and the falloff spectral shapes at both low and high frequencies. The spectra have different widths, from the narrowest for the low-frequency component to the widest for the high-frequency component, reflecting the different size distributions of the three groups of landing gear parts. The wheels have the same size so that the low-frequency noise from the wheels is narrowly confined to frequencies near the vortex shedding frequencies of the wheels. For noise from the main struts that have various sizes, the spectrum has a broad hump. The spectral hump becomes even broader for the high-frequency noise because many different sizes are included in the group of small features that generate high-frequency noise. Directivity factors will also be presented for all three noise components, which have minima at 90° of emission angle and higher values at other angles with maxima in the upstream and downstream directions. The angular variations are greatest for the high-frequency components and almost flat for the low-frequency noise.

The amplitude of each of the three noise components will be determined by geometric and flow quantities unique to the corresponding group of landing gear parts, together with functional dependencies that are common to all three components. The common features are the Mach number dependence, the spherical spreading, the convective amplification and the atmospheric absorption. For landing gear noise that is usually at low Mach numbers, the dominant noise sources are the pressure fluctuations on the surfaces of the landing gear parts, according to the theory of aerodynamic sound [9–13]. Thus, the noise levels depend on the aggregate effects of surface integrations of the surface pressures. Because of the significant variations in the dimensions of gear parts, the functional dependencies of the noise levels on the surface integration effects are inevitably component dependent. For the low- and mid-frequency component, this effect will be deterministically defined by the dimensions of the wheels and main struts, respectively. For the high-frequency noise associated with small geometric features in the gear assembly, the large number of irregularly shaped parts makes it impractical to count and define the sizes and shapes of all the small parts. Thus, we will introduce a complexity factor to account for the small parts, which can be regarded as a statistical description of the sources of high-frequency landing gear noise. We will discuss geometric and flow parameters that affect this complexity factor and an empirical definition will be given for practical applications.

To validate the prediction schemes and demonstrate their practical applications, the prediction models developed here will be applied to the main landing gear noise of the Boeing 737 aircraft. The predictions will be compared with wind tunnel test data for an isolated main landing gear, at various flow conditions and emission angles. The comparisons between predictions and data show good agreements; the models not only capture the parametric trends of the noise measurements, but also accurately predict the absolute noise levels.

2. Theoretical basis and scaling laws

Our prediction models for landing gear noise are based on the scaling laws of the theory of aerodynamic noise generation. The general theory of sound generation by moving bodies has been extensively studied in the past [10–13], so that only the main results are briefly derived here for the convenience of discussions, with particular reference to landing gear noise [9]. We consider a landing gear assembly moving at constant speed U in the positive x_1-direction, where the coordinate system $\mathbf{x} = \{x_1, x_2, x_3\}$ is fixed in relation to the far-field microphones. The geometry and coordinate system are illustrated in Fig. 1. By starting with the Ffowcs Williams/Hawking equation [10], making the far-field approximation and taking Fourier transform from time to frequency domain, the acoustic pressure in the far field can be derived as

$$\tilde{p}(\mathbf{x},\omega) = \frac{ik_0\hat{x}_i}{4\pi R}e^{ik_0R}\int_{S(\boldsymbol{\eta})} n_i\tilde{p}_s(\boldsymbol{\eta},\omega_d)e^{-ik_0\boldsymbol{\eta}\cdot\hat{\mathbf{x}}}\,d^2\eta. \tag{1}$$

Here, p denotes the pressure fluctuations, with the overhead tilde indicating quantities in the Fourier transform domain and the subscript s for quantities on the surface of the landing gear parts. This result relates

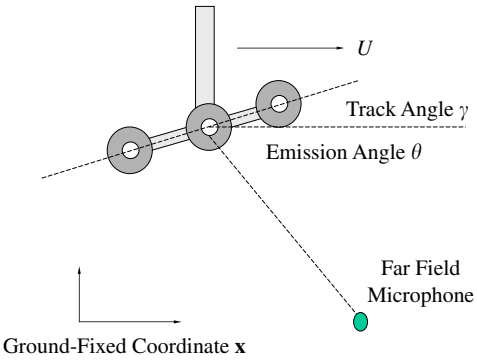

Fig. 1. Illustration of the landing gear geometry and definitions of the coordinate system.

the far-field sound pressure at angular frequency ω to the surface pressures at the Doppler-shifted frequency ω_d. This shift in frequency between the surface pressures and the far-field sound pressure is due to the effects of the motion of the gear, with velocity $\mathbf{U} = U\hat{x}_1$ in the x_1-direction, the overhead hat on x_1 denoting unit vector. The Doppler-shifted frequency is defined by $\omega_d = \omega\Delta$ with Δ standing for the Doppler factor defined by

$$\Delta = 1 - \frac{\mathbf{U}\cdot\mathbf{x}}{c_0|\mathbf{x}|} = 1 - M\hat{x}_1 = 1 - M\cos\theta, \tag{2}$$

where $M = U/c_0$ denotes the Mach number with c_0 being the constant sound speed and we have introduced the emission angle θ which is measured from the upstream direction of the flight path, as illustrated in Fig. 1. In Eq. (1), we have also used $k_0 = \omega/c_0$ to denote the acoustic wavenumber and R the distance of the far-field microphone from the landing gear. The surface integration is on all the surfaces of the landing gear parts, collectively denoted by S with the surface coordinates denoted by $\boldsymbol{\eta}$. The unit normal of the surface, pointing into the flow, is denoted by n_i, with the repeated indices implying tensor summation.

The noise spectrum (power spectrum density) can be derived from the far-field pressure by multiplying it by its complex conjugate and taking the ensemble average of the result. By denoting the noise spectrum by Π, we have the definition

$$\Pi(\mathbf{x},\omega)\delta(\omega-\omega') = \left\langle \tilde{p}(\mathbf{x},\omega)\tilde{p}^*(\mathbf{x},\omega')\right\rangle, \tag{3}$$

where the asterisk denotes complex conjugate, δ is the Dirac delta function, and the bracket $\langle \ldots \rangle$ implies ensemble average. From this, a trivial integration with respect to ω' leads to

$$\Pi(\mathbf{x},\omega) = \int_{\omega'} \left\langle \tilde{p}(\mathbf{x},\omega)\tilde{p}^*(\mathbf{x},\omega')\right\rangle \mathrm{d}\omega'. \tag{4}$$

By substituting the far-field sound pressure equation (1) into this, we have

$$\Pi(\mathbf{x},\omega) = \frac{\hat{x}_i\hat{x}_j}{(4\pi R)^2}\int_{S'}\int_S n_i n'_j \int_{\omega'} kk' \mathrm{e}^{\mathrm{i}(k_0-k'_0)R}\left\langle \tilde{p}_s(\boldsymbol{\eta},\omega_d)\tilde{p}_s^*(\boldsymbol{\eta}',\omega'_d)\right\rangle \mathrm{e}^{\mathrm{i}(k'_0\boldsymbol{\eta}'-k_0\boldsymbol{\eta})\cdot\hat{\mathbf{x}}}\,\mathrm{d}\omega'\,\mathrm{d}^2\eta\,\mathrm{d}^2\eta'. \tag{5}$$

The integration with respect to ω' can be carried out by making use of Eq. (3) applied to the surface pressures, leading to

$$\Pi(\mathbf{x},\omega) = \frac{k_0^2\hat{x}_i\hat{x}_j}{(4\pi R)^2\Delta}\int_{S'}\int_S n_i n'_j \Pi_s(\boldsymbol{\eta},\boldsymbol{\eta}',\omega_d)\mathrm{e}^{\mathrm{i}k_0(\boldsymbol{\eta}'-\boldsymbol{\eta})\cdot\hat{\mathbf{x}}}\,\mathrm{d}^2\eta\,\mathrm{d}^2\eta', \tag{6}$$

where Π_s is the cross-power spectrum density of the surface pressure fluctuations.

By the definition of mean square pressure fluctuations, we can now integrate the power spectrum density equation (6) within a particular frequency band to derive

$$\left\langle p^2\right\rangle = \frac{1}{2\pi}\int_\omega \Pi(\mathbf{x},\omega)\,\mathrm{d}\omega, \tag{7}$$

where the mean squared pressure on the left-hand side is to be understood as that for a particular frequency band and the integration with respect to ω on the right-hand side is performed over that band. Thus, the result is a function of the center frequencies of the frequency bands. By substituting Eq. (6) into this, we find that

$$\langle p^2 \rangle = \frac{2\hat{x}_i\hat{x}_j}{(4\pi)^3 c_0^2 R^2 \Delta^4} \int_{S'} \int_S n_i n'_j \int_{\omega_d} \omega_d^2 \Pi_s(\boldsymbol{\eta}, \boldsymbol{\eta}', \omega_d) e^{ik_0(\boldsymbol{\eta}'-\boldsymbol{\eta})\cdot\hat{\mathbf{x}}} \, d\omega_d \, d^2\eta \, d^2\eta'. \tag{8}$$

Here, again, the integration with respect to ω_d on the right-hand side is performed over a set of frequency bands so that the result is a function of the center frequencies of those bands. The 1/3 octave frequency bands can be a convenient choice. In cases where atmospheric absorption is to be included in the prediction, it is more suitable to choice narrow bands to define Eq. (8), because of the significant variations of atmospheric absorption with frequency. This definition is followed here and the 1/3 octave band mean square pressure fluctuations will be computed by standard integration after the atmospheric absorption is applied to the narrow band results.

The analytical result equation (8) can be further reduced by dimensional analysis to derive scaling laws for the use of empirical prediction. To this end, we define a typical length scale ℓ_0, time scale τ_0, and velocity scale u_0, which are related to each other by

$$\ell_0 = u_0 \tau_0. \tag{9}$$

The velocity scale u_0 characterizes the unsteady motions of the flow and is usually different from the uniform velocity U of the moving landing gear. With these scaling parameters, we can define the Strouhal number by

$$St = f\ell_0/U = \omega\ell_0/(2\pi U), \tag{10}$$

where f denotes frequency and ω is the angular frequency, as defined before.

The cross-spectrum density of the surface pressures is determined both by its amplitudes and by the coherence length of the cross-spectrum. The former sets the scaling of the cross-spectrum and the latter specifies the domain of significant contributions in the surface integrations in Eq. (8). Its amplitude can be scaled as

$$\Pi_s \sim (\rho_0 u_0^2)^2 \tau_0, \tag{11}$$

where ρ_0 is the constant mean density. Experimental studies in the past have shown that surface pressure fluctuations generated by unsteady flows are almost always orders of magnitudes smaller than the dynamic pressure of the mean flow ($\rho_0 U^2/2$). This means that the velocity scale u_0 defined here is much smaller than the mean flow velocity U.

Because the cross-spectrum of the surface pressures is nonzero only within the coherent length, which is typically of the same order as ℓ_0, the double surface integration in Eq. (8) is controlled by both the surface dimension of the gear parts and the coherence length scale. Thus, the double surface integration should be normalized by

$$d^2\eta \, d^2\eta' \sim \ell_0^2 S, \tag{12}$$

where S denotes the typical area of the body surface.

The terms in Eq. (8) that involve the scalar product of the far-field location unit vector and the unit normal of the integration surface give the directivity of the generated noise. Thus, we can scale these terms as

$$\hat{x}_i \hat{x}_j n_i n'_j \sim D(\theta, \varphi), \tag{13}$$

where D denotes the far-field directivity, which is in general a function of the emission angle θ in the flyover plane and the azimuthal angle φ at side line locations. The former is important for aircraft noise certification at landing conditions, which is why most of the available data are for these angles, and the latter is usually used in airport noise map studies. Owing to the availability of test data, the directivity models presented here will be only for emission angles in the flyover plane.

By normalizing the quantities in Eq. (8) with the scaling laws discussed above, we can rewrite the result as

$$\langle p^2 \rangle = (\rho_0 c_0^2)^2 M^6 D(\theta) \beta e^{-\alpha R} F(St) \frac{S}{R^2} \frac{1}{(1 - M\cos\theta)^4}, \tag{14}$$

where we have introduced the new quantities α, β, and F to denote, respectively, the attenuation due to atmospheric absorption, the radiation efficiency due to the production of unsteady flows by the steady motion of the landing gear and the normalized spectrum of the radiated noise. The first of these new quantities, α, is defined by decibels per length and is a function of frequency. For practical applications where the propagation distance is usually many wavelengths, atmospheric absorption can significantly affect the amplitude of the noise received by the far-field microphones so that it is included here. The second quantity, denoted by β, is essentially a radiation efficiency factor. It is defined by

$$\beta = u_0^3/(4U^3). \tag{15}$$

This measures the efficiency of energy conversion from the steady motion U of the body to the unsteady flows characterized by u_0. It can be noted that the scaling of this quantity on the third power of the characteristic velocity of the unsteady flow results from the parametric dependence of the surface pressure cross-spectrum on this velocity, as specified in Eq. (11). The third quantity, the normalized spectrum F, is a function of the Strouhal number St defined by Eq. (10). Mathematically, this normalized spectrum is simply written for the integrals in Eq. (8), namely,

$$F = \int_{S'}\int_{S} \frac{\hat{x}_i\hat{x}_j n_i n'_j}{D(\theta,\varphi)} \int_{St_d} St_d^2 \frac{\Pi_s(St_d)}{(\rho_0 u_0^2)\tau_0} e^{ik_0(\boldsymbol{\eta}'-\boldsymbol{\eta})\cdot\hat{\mathbf{x}}}\, dSt_d \frac{d^2\eta\, d^2\eta'}{\ell_0^2 S}. \tag{16}$$

Since all quantities in this expression have been normalized with respective typical parameters, they should all have values of the order of unity at its maxima. The normalized spectrum should thus also be of the order of unity. Clearly, the calculation of this spectrum requires detailed information on the surface pressure spectrum, which is usually not available in practical applications. For our empirical methods, this normalized spectrum will be modeled and calibrated by test data, which will be discussed in detail in the following sections.

The derivations that lead to the scaling law equation (14) show that it is a general result applicable to any individual parts in the landing gear assembly, from the largest parts, the wheels, to the smallest dressings. The functional dependencies of the far-field noise on the geometric and flow parameters are summarized in Table 1. It is evident that some of the parametric dependencies are common to all parts. These include the dependence on ambient parameters, the sixth power law for Mach number, the spherical spreading of the noise, the convective amplification and the atmospheric absorption. The other functional dependencies in Eq. (14), such as the normalized spectrum, the radiation efficiency, the far-field directivity and the surface of the integration, are component specific and may vary significantly. These component-specific quantities are also the ones that are difficult to define quantitatively, either by experimental studies or by analytical/numerical calculations, essentially because of the variations in shapes, sizes and locations of the large number of parts in the gear assembly. These parametric dependencies can only be modeled empirically by correlating the scaling laws to experimental data.

Even in such an empirical approach, it is apparently very difficult to individually model every part in the gear assembly that generates noise, which is a main reason why we follow the approach of cataloging the gear parts into three basic groups and decomposing the landing gear noise spectrum into three corresponding

Table 1
Functional dependencies of landing gear component noise

Feature	Dependency
Ambient medium	$(\rho_0 c_0^2)^2$
Mach number	M^6
Spherical spreading	R^{-2}
Convective amplification	$(1-M\cos\theta)^{-4}$
Atmospheric absorption	$e^{-\alpha R}$
Directivity	$D(\theta)$
Radiation efficiency	β
Component size effect	S
Spectrum	$F(St)$

spectral components. The development of this model will be discussed in detail in the following sections. Clearly, it reduces the empirical modeling to three components, instead of all the individual parts in the gear assembly. The latter approach is in principle feasible [4,5,8], where the total landing gear noise is predicted by building up the noise from the individual parts.

3. Spectral decomposition

Our prediction schemes start with the hypothesis that landing gear noise can be decomposed into three spectral components, respectively, for the low-, the mid- and the high-frequency domain, and the total noise is the incoherent energy summation of the three components. This enables us to express the total landing gear noise as

$$\langle p^2 \rangle = \langle p_L^2 \rangle + \langle p_M^2 \rangle + \langle p_H^2 \rangle, \tag{17}$$

where the subscripts L, M, and H, respectively, indicate the low-, the mid- and the high-frequency component. This spectral decomposition has been discussed in detail before [7–9]. It results from a combination of data analyses of recent landing gear noise tests and source mechanisms of the noise. Full configuration landing gear noise tests have shown that the far-field noise has different spectral features and directivity characteristics in different frequency domains (also see Ref. [15]). This has been attributed to the noise generated by the three groups of landing gear parts, namely, the wheels, the main struts and the small details. The three groups have significantly different typical sizes, which makes their dominant noise well separated from each other in frequency.

With the spectral decomposition equation (17), we can apply the result in Eq. (14) to each of the three components. The normalized spectrum F is now defined as a function of the Strouhal number, based on the respective length scales in each spectral component. We choose the diameter of the wheels d, the average cross-section dimension of the main struts a and the typical size of the small details ℓ as the length scales of, respectively, the low-, the mid- and the high-frequency component. With this, the total landing gear noise can be written as

$$\langle p^2 \rangle = \frac{(\rho_0 c_0^2)^2 M^6 \mathrm{e}^{-\alpha R} D_0(\theta)}{R^2 (1 - M\cos\theta)^4} \{P_L + P_M + P_H\}, \tag{18}$$

where features common to all components have been factored out and those that are component-specific are represented by the quantity P, with respective subscripts for the three components. They are defined by

$$P = \beta S D(\theta) F(St). \tag{19}$$

Here, the respective subscripts L, M, and H should be used for all quantities to indicate the low-, the mid- and the high-frequency component. The Strouhal number for each component is also defined by the corresponding characteristic length of each component. These results indicate that all three spectral components have their own individual directivity, but we have also included a directivity factor in Eq. (18), denoted by $D_0(\theta)$, to account for the installation effects. Thus, the directivity factors in Eq. (19) are for isolated landing gears for the individual spectral components and that in Eq. (18) accounts for the wing/fuselage reflection and other installation effects.

With the results given in Eqs. (18) and (19), it only remains to model the quantities on the right-hand side of Eq. (19), respectively, for the three frequency domains. This will be done by a combination of physical reasoning and calibration with test data. The flow energy conversion efficiency, denoted by β, with respective subscripts for the three spectral components, can only be derived by matching predictions with test data, though it is derived to basically describe how efficiently the motion of the landing gear generates unsteady flows, characterized by the velocity scale u_0, which in turn radiates noise. Apparently, this quantity is not only related to the structural design of the gear assembly, but also depends on the relative locations of the gear components. An example is the variations of landing gear noise with the alignment angle of the wheel track (see Fig. 1 for the definition of wheel alignment angle) with respect to the flight direction. It has been observed that, for the Boeing 777 aircraft, a noise reduction of 2–3 dB in a broad frequency range can be achieved by reducing the wheel track alignment angle from the conventional operational angle of 13° to zero, making the

wheel track align with the flow. This indicates the aerodynamic coupling of the noise-generating components in the gear. This aerodynamic coupling of the landing gear sources is clearly difficult to study, but should be included in practical predictions, whenever enough information is available for practical models to be established. Thus, we propose the model for this quantity in the form of

$$\beta = \beta_0 \left[1 + 4 \frac{N_w - 2}{N_w} \sin(2\gamma) \right], \tag{20}$$

where N_w is the number of wheels in the gear assembly and γ denotes the gear track alignment angle, measured from the flow direction. Values for the empirical constant are given in Table 2 for the three spectral components and for both main and nose gears. The need for different sets of values for the two types of gears and the derivations of the values for the nose gears are given in Ref. [27]. The effects of the wheel alignment angle on the noise levels are illustrated in Fig. 2, which plots the noise level increments as a function of the wheel track angle. It should be emphasized that the empirical model for the wheel track angle effects is basically calibrated by limited test data of the Boeing 777 main landing gear. The trends shown by these limited data are by no means conclusive. Further studies in this regard are clearly needed and the simple empirical model used here should be considered only as a first attempt and a place holder for the wheel track angle effects.

The amplitude of each noise component is related to the aggregate surface area of the landing gear parts in each group, resulting from the surface pressure integration of the basic theory equation (8) and denoted by S with respective subscripts for the three spectral components. For the low-frequency noise that is generated by the wheels, it is denoted by S_L and can be derived deterministically from the wheel dimensions. This leads to

$$S_L = \pi N_w d, \tag{21}$$

where N is the number of wheels in the landing gear assembly, w the wheel width and d the diameter. It is clear that Eq. (21) does not account for the side surfaces of the wheels, because the normal of those surfaces is approximately perpendicular to the far-field location vector in the flyover plane so that their noise contributions are negligible. The wheel diameter d is also used as the length scale for the low-frequency noise, which defines the Strouhal number in the frequency domain according to

$$St_L = fd/U. \tag{22}$$

For the mid-frequency component that is associated with the main struts in the landing gear, the aggregate effect of the surface pressure integration is denoted by S_M and can be computed as the summation of the

Table 2
Empirical amplitudes of the three landing gear noise components, as defined by β_0 in Eq. (20)

	Low	Mid	High
Main	2.3×10^{-8}	7.5×10^{-9}	1.6×10^{-5}
Nose	2.3×10^{-8}	6.0×10^{-9}	0.8×10^{-5}

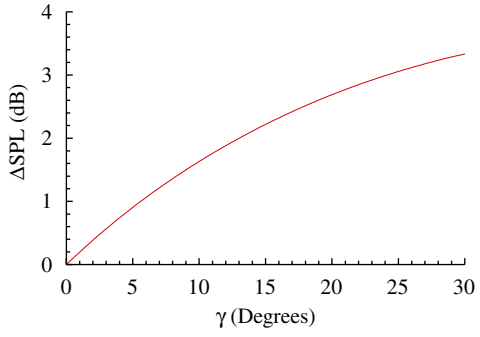

Fig. 2. Increment of landing gear noise due to wheel track alignment angle.

surface areas of the main struts. The main struts are defined here as the elongated parts whose lengths are much larger than their cross-section dimensions. They include the axles connecting the wheels, the shock struts connecting the wheel track to the aircraft, the side bars attached to the shock struts and the main hydraulic components. Under this definition, the surface of an individual part is the perimeter of the cross-section multiplied by its length. For structural strength purpose, the main struts are usually designed with cross-sections of either circular shape or rectangular shape. Though the struts of rectangular cross-sections usually have cutouts so that they look more like I-beams or other cross-sections, we will regard all non-circular struts as rectangular for simplicity, and account for the effects of cutouts and other irregularities in the high-frequency components. Thus, we can define

$$S_M = \sum_{j=1}^{N_s} s_j L_j, \tag{23}$$

where s_j is the perimeter of the cross-section of the jth strut, L_j is its length and N_s is the total number of main struts in the landing gear assembly. The perimeter of the cross-section is defined by

$$s_j = \begin{cases} \pi d_j & \text{for circular cross-section,} \\ 2(a_j + b_j) & \text{for non-circular cross-section,} \end{cases} \tag{24}$$

where d_j is the diameter of the cross-section if the jth strut is circular and a_j and b_j are its two linear dimensions if it is non-circular. The total length of the struts, denoted by L, is simply

$$L = \sum_{j=1}^{N_s} L_j. \tag{25}$$

The average dimension of the cross-sections of the main struts is given by

$$a = S_M/(\pi L). \tag{26}$$

It can be seen that this is a weighted average, taking into account the variations in the lengths of the struts. This is the quantity that is used as the length scale to define the mid-frequency Strouhal number, namely,

$$St_M = fa/U. \tag{27}$$

It can be noted that the total number of main struts for the mid-frequency noise component is not precisely defined, which for practical applications is not a significant uncertainty. The guideline is to include all large parts in the gear assembly, except the wheels, which are much larger in size than the small details. The latter is defined as those small parts such as brake braces, hydraulic hoses, and wires, as well as small geometry irregularities such as cutouts and steps. Apparently, there is no clear-cut definition as to what to include in this group of parts, but for practical applications, this poses no difficulty. As long as the large struts are included, the noise amplitude, proportional to the summation equation (25), will not be significantly affected by the addition of a few small parts.

For the high-frequency component, the surface area calculation can in theory be carried out in a way similar to those used for the other two components, but this is clearly not practical, because of the large number of small parts and irregular geometric features in the gear assembly, which always have very different sizes, shapes and orientations. Thus, the aggregate effect of the surface integration for high-frequency noise can only be modeled as a statistical quantity. The modeling of this quantity depends on the complexity of the small features in the landing gear, both the amount of small details and the relative locations of the small parts. To account for effects such as these, we model the aggregate surface integration effects in the high-frequency domain as

$$S_H = \eta \ell^2, \tag{28}$$

where the length scale of the high-frequency noise sources is denoted by ℓ and we have introduced a non-dimensional quantity, the complexity factor η, to account for the geometric complexity of the large number of small parts in the landing gear. This quantity will be discussed and defined in detail in a later section.

The length scale of the high-frequency noise source is used in Eq. (28) to reconcile the dimension of the surface quantity S_H. It is, however, an important parameter to define the Strouhal number in the high-frequency domain,

$$St_H = f\ell/U. \tag{29}$$

For a given mean flow velocity, the length scale ℓ determines the frequency of the maximum high-frequency noise, which in turn affects the levels of the total noise in the high-frequency domain. This length scale can be taken as the typical size of the small geometric features in the landing gear, the average of the dimensions of the small features, for example. The small features include dressings attached to the main struts, standing-along parts such as brake braces, hydraulic hoses and wires, and small geometry irregularities such as cutouts and steps. Though a detailed survey is feasible to measure the sizes of the small features, it is by no means a trivial task, considering the large number of small details involved. It is then desirable to predefine a simpler way to obtain this length scale. In examining practical landing gears, we noticed that the sizes of the small details vary with the sizes of the large parts such as the main struts. Thus, we define the high-frequency length scale simply by

$$\ell = 0.15a, \tag{30}$$

where a is the length scale for the mid-frequency noise, defined by Eq. (26) as the length-weighted average dimension of the cross-sections of the main struts. Using this definition, the task of measuring the large number of small details is avoided.

4. Normalized spectra

The normalized spectra describe the frequency features of the landing gear noise in the three frequency domains. They are, respectively, determined by the three different noise-generating groups of parts in the landing gear assembly, and each of them has its unique spectral characteristics. There are also general features that are common to all three components. They all achieve their maximum of unity at a value of the Strouhal number that characterizes the noise generation mechanisms, and they all fall off on both sides of the maximum at low and high Strouhal numbers. The falloffs have different rates for different spectral components. To accommodate features like these, a general form can be proposed for the normalized spectrum

$$F(St) = A\frac{St^{\sigma}}{(B + St^{\mu})^{q}}, \tag{31}$$

where the indices σ, μ, and q are empirical constants, which jointly define the spectral shape of the normalized spectrum, and A and B are parameters to ensure that F assumes its maximum of unity at a value of the Strouhal number. We assume this general form for all three spectral components, but when applied to a particular component, a corresponding subscript should be used for the symbols.

Once the empirical constants σ, μ, and q are given, by fitting with experimental data, for example, the parameters A and B can be determined analytically. By taking the derivative of the normalized spectrum F with respect to the Strouhal number St, it is straightforward to show that

$$\frac{\mathrm{d}F}{\mathrm{d}\,St} = \frac{A\,St^{\sigma-1}}{(B + St^{\mu})^{q+1}}\{\sigma(B + St^{\mu}) - q\mu\,St^{\mu}\}. \tag{32}$$

To require that the spectrum achieves maximum at the Strouhal number

$$St = St_0, \tag{33}$$

we can set the derivative equation (32) to zero at this Strouhal number, which in turn leads to the vanishing of the terms inside the brackets. This determines the value of B as

$$B = \{(\mu q/\sigma) - 1\}St_0^{\mu}. \tag{34}$$

The parameter A can now be determined by setting F to unity at the Strouhal number equation (33), which, after some straightforward algebra, leads to

$$A = (q\mu/\sigma)^{q}St_0^{q\mu-\sigma}. \tag{35}$$

The above discussions analytically determine the parameters A and B in terms of the indices μ and q and the value of St_0 which themselves need to be derived empirically. By analyzing trends in test data and curve fitting the data, we find a set of values for these parameters, listed in Table 3 for all three noise components, together with those of A and B calculated by using Eqs. (34) and (35). These values completely define the normalized spectra. For illustration, some examples of the three normalized spectra are plotted in Fig. 3 as a function of frequency in the range between 50 and 10,000 Hz, which is the frequency range of interest for aircraft noise. In the examples, the flow Mach number is taken as 0.2 and the three length scales d, a, and ℓ are, respectively, 40, 4, and 0.6 in, respectively, corresponding to 1.016, 0.106, and 0.01524 m). The last, namely, the length scale for the high-frequency noise, is calculated according to Eq. (30). The common features of the spectra are the unity maximum at the peak Strouhal number, and the falloff on both sides of the maximum for both low and high values of Strouhal numbers. Since the three spectral components have different length scales, the spectral maximums are achieved at different frequencies. Also because of the three different length scales, the three spectra cover a wide range of frequencies.

The shapes and falloffs of the normalized spectra are controlled by the parameters, given in Table 3. From Eq. (31), it is clear that the low Strouhal number dependence of the spectrum is given by

$$F(St) \sim St^{\sigma} \quad \text{for} \quad St \ll St_0 \tag{36}$$

and at large Strouhal numbers, the falloff follows:

$$F(St) \sim St^{-(q\mu-\sigma)} \quad \text{for} \quad St \gg St_0. \tag{37}$$

Since noise spectrum decreases at low and high frequencies away from the spectral maximum, the result equation (37) imposes a condition on the values of the indices, namely,

$$q\mu > \sigma. \tag{38}$$

Clearly, both are satisfied by the values given in Table 3.

The parameters μ and q also jointly define the width of the spectrum near the maximum frequency. It can be seen from Fig. 3 that the low-frequency component has the narrowest width and the high-frequency

Table 3
Parameters to define the normalized spectra for the three landing gear noise components

	Low	Mid	High
St_0	1.0	0.3	0.1
σ	4.0	3.0	2.0
μ	2.5	1.5	1.1
q	2.6	4.2	4.2
A	3.53	0.42	0.08
B	0.62	0.18	0.10

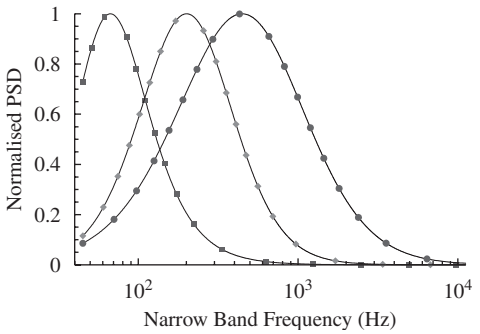

Fig. 3. Illustration of the normalized power spectral density for the three spectral components with the symbol squares, diamonds and circles, respectively, representing the low-, mid- and high-frequency component.

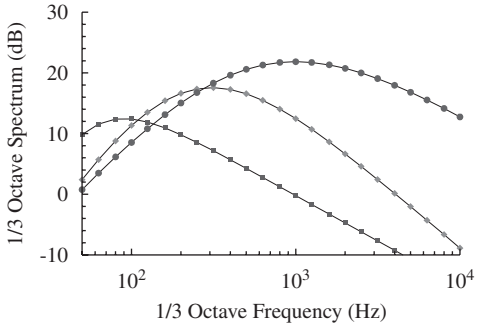

Fig. 4. One-third octave band spectra of the three power spectral densities shown in Fig. 2 with the symbol squares, diamonds and circles, respectively, representing the low-, mid- and high-frequency component in Fig. 3.

component has the widest width with the mid-frequency component in between the two. This means that the low-frequency noise is narrow banded and the noise becomes more broad banded as frequency increases. This reflects the source physics of the three noise components and can be simply explained by the length scales of the three groups of landing gear parts that generate noise, respectively, in the three frequency domains. For the low-frequency noise that is related to the wheels, there is only one size, namely, the wheel dimension, so that the noise spectrum is narrowly confined to frequencies near the vortex shedding frequencies of the wheels. In the mid-frequency domain, the parts that generate noise are the main struts which have a variety of sizes. Each of the struts may still radiate noise near its characteristic frequency, determined by the Strouhal number similarity rule, but the aggregate effects of the group of parts cover a range of frequencies, making the spectrum more broad banded than a single part. The spectrum is even more broadened in the high-frequency domain because the size distribution of the small parts in the landing gear covers an even wider range. The normalized spectra defined by Eq. (31) lead to broadband 1/3 octave band sound pressure levels (SPLs). This is demonstrated in Fig. 4, where the 1/3 octave band results are simply integrated from the narrow band spectra plotted in Fig. 3. The higher levels for the high-frequency component result from the progressively wider 1/3 octave band width as frequency increases.

5. Directivity factors

Test data have shown that noise from isolated landing gear in general follows a directivity pattern that peaks at the upstream and downstream direction and achieves minimum near the flyover location where the emission angle is approximately 90° (e.g. Refs. [7,15]). This has also been observed in numerical simulations of landing gear noise using simple gear models [22–26]. Detailed analyses of test data further reveal that the variations of far-field noise with emission angle are also frequency dependent. At low frequencies, the variations are very small and the radiation is almost omni-directional. As frequency increases, the radiation becomes more directional, showing variations of a few decibels in the mid- and high-frequency domain.

To account for this frequency-dependent directivity, a general form is assumed for the directivity factor for the three spectral components

$$D(\theta) = (1 + h\cos^2\theta)^2, \tag{39}$$

where h is an empirical constant whose values are listed in Table 4 for the three landing gear noise components. When this general form is applied to a particular component, with corresponding values for the empirical constant, a subscript, L, M, or H, should be used to identify the noise component, namely, the low, the mid or the high-frequency component. The three directivity factors are plotted in Fig. 5, as a function of the emission angle θ. The general features are that all three components have maxima in the upstream and downstream direction and minima at the flyover location at emission angle of 90°. The differences between them are the amount of variations with emission angle. For the low-frequency component, the variations are the smallest among the three, representing essentially omni directional radiation. The variations for the mid and high-frequency component are more noticeable.

Table 4
Parameters defining the directivities of the three landing gear noise components

Component	Low	Mid	High
H	0.2	0.6	1.0

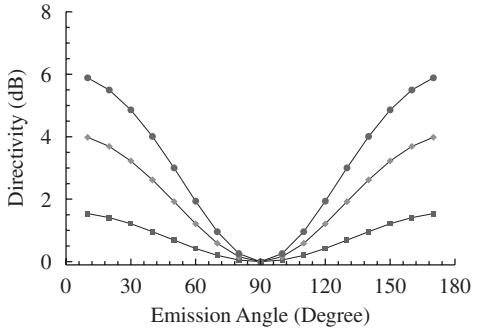

Fig. 5. Models of the directivity factors for the three spectral components of landing gear noise with the symbol squares, diamonds and circles, respectively, representing the low-, mid- and high-frequency component.

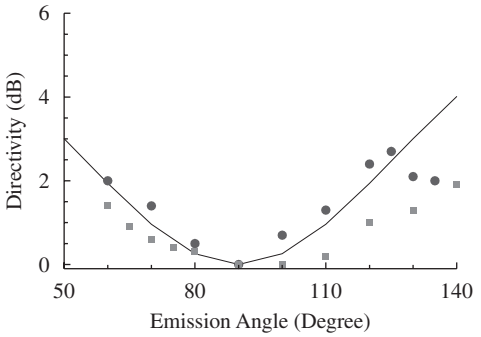

Fig. 6. Comparison of empirical model with test data for the directivity of high-frequency landing gear noise. The curve is the prediction and the symbol squares and circles are test data, respectively, for the Boeing 737 and the Airbus 320 aircraft.

These parametric trends are all empirically modeled and are all consistent with test data, including both isolated landing gears in wind tunnel tests and flight tests with full configuration aircraft. To demonstrate, the high-frequency noise directivity is compared in Fig. 6 with test data for the range of emission angle covered by the test data. The solid curve in this figure is the empirical model defined by Eq. (39) and the symbols are data, with the squares for the Boeing 737 two-wheel gear [7,16] and the circles for the Airbus 320 four-wheel gear [15]. Both data sets are from wind tunnel tests and the details of the tests are described in the respective references. The Boeing 737 data are for the frequency domain from 1000 to 13,000 Hz, and the A320 data are for a range of Strouhal number from 4 to 12. In the latter case, the definition of the Strouhal number is given in Ref. [15] and the range of 4–12 is described as the high-frequency domain. Clearly, the comparison between the empirical model and the data shows good consistency.

The above discussions on the directivity variations of the three spectral components apply to isolated gears without the installation effects due to the reflection/diffraction from the aircraft wing and fuselage. The variations account for the directivities of individual sources, which are only one of the three elements that determine the overall far-field noise directivity. The other two are the convective amplification, as already included in the model equation (18), and the installation effects. Thus, it only remains to model the installation effects to complete the modeling of far-field directivity of the landing gear noise. There are only limited flight data available that can be used to extract the installation effects and there have been almost no studies on this

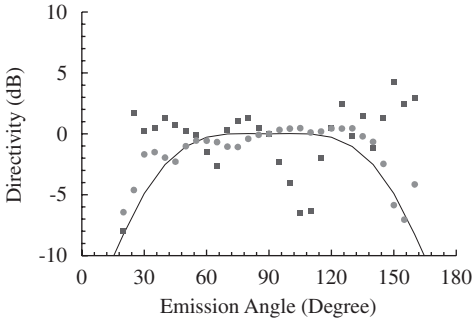

Fig. 7. Comparison of overall far-field directivity between prediction and test data for the Boeing 777 landing gear noise with the curve being the prediction and the symbols squares and circles representing test data for the Boeing 777-300 and 777-200 aircraft, respectively.

by other approaches such as numerical simulations. Thus, once again, we will develop an empirical model from physical reasoning and calibration with available data. Intuitively, it is easy to see that the aircraft wing/fuselage reflection and diffraction will enhance the far-field noise and this enhancement will be maximal at the overhead location and minimal in the flight direction. It is also clear that the maximum increase in far-field noise due to the installation effects will be less than 3 dB, which would be achieved only from complete reflection of an infinite plate. To capture all these, we model the installation effects by

$$D_0(\theta) = 1.2 \times (1 - 0.9\cos^2\theta)^2. \tag{40}$$

This gives about 0.8 dB of noise increase at the overhead location of 90° of emission angle and the increase becomes negligible in the flow direction. The amount of noise increase at the overhead location in this model is entirely empirical, based only on the physical argument that the aircraft wing and fuselage provides some reflection and diffraction. We believe that this small amount of increase is reasonable for practical applications, though more detailed studies will be needed to define it more accurately.

Before detailed studies on the installation effects are available, the empirical model equation (40) can only be calibrated by test data. An example of such a calibration is shown in Fig. 7, by using some flight test data of the Boeing 777 aircraft. As discussed before, the overall landing gear noise directivity contains three elements, the directivities of the individual sources, the convective amplification due to the motions of the sources and the installation effects. Since the Boeing 777 landing gear noise is dominated by the high-frequency component, we plot the quantity

$$(1 - 0.9\cos^2\theta)^2(1 + h_H\cos^2\theta)^2 \tag{41}$$

as the overall directivity, with h_H given in Table 4. The flight test data are processed by extracting the convective amplification from the data and normalizing the results by the level at 90° of emission angle. The empirical model seems to captures the trends of the far-field noise pattern. The test data show significant scatter because the data were derived by subtracting the airframe noise, measured with landing gears retracted, from the total airframe noise, with both landing gears and other noise generating devices. This procedure usually works well in cases where the contributions from the two differ significantly, but involves uncertainties when the two are comparable. The latter is unfortunately the case.

6. Complexity factor

To account for the large number of small features in the landing gear assembly, which is the source of high-frequency noise, we have introduced a complexity factor in the empirical method, used in Eq. (28) to define the aggregate effects of surface integration over the surfaces of all the small parts. The qualitative description of this complexity factor is that it correlates the noise with the geometric complexity of the landing gear. The more complicated the landing gear assembly, the higher the noise levels. The geometric complexity of the landing gear is of course difficult to define quantitatively and uniquely. It can be related to aircraft operational

Table 5
Examples of maximum gross takeoff weight for some aircraft types

Aircraft	Max. takeoff weight (lb)	Max. takeoff weight (N)
717	110,000	493,042
737	150,000	672,330
747	840,000	3,765,048
757	260,000	1,165,372
767	420,000	2,882,524
777	650,000	2,913,430

parameters such as the takeoff gross weight, or aerodynamic quantities such as the total drag of the landing gear, or the geometry of the gear such as its wheels and struts and their relative locations.

The aerodynamic parameters are attractive in relating the noise to its sources. The correlation of the complexity factor with the total drag of the landing gear is one way to define the complexity factor, because more complex landing gears correspondingly produce both more noise and more drag, because of the small, irregular geometric features. The drawback of this approach is that the total drag of a landing gear is not an easy quantity to obtain. In most cases, it has to be measured in wind tunnel tests. For this reason, we will not follow this approach, but will define the complexity factor from quantities that are easy to obtain from the landing gear geometry and the aircraft operation conditions.

It is easy to see that a significant source of geometric complexity, and hence, of landing gear high-frequency noise, comes from the brake systems of the wheels, which are attached to the inner sides of the wheels with various parts of very irregular shapes and sizes. Since each wheel is equipped with such a system, the complexity factor for high-frequency noise prediction can be assumed to increase with the number of wheels in the gear assembly. The more wheels the gear has, the more brake systems it needs, which in turn radiate more noise. The same reasoning applies to the main struts. There are hardly any clean struts in practical landing gears; most of them have cutouts and steps and they are almost always attached with braces, cables and wires. Thus, the more struts the gear assembly has, the more small details it has, and hence, the more noise it generates. The complexity factor for noise prediction can then be assumed to also increase with the total length of the main struts.

There are of course geometric features that are not directly attached to the wheels and struts, hydraulic and cabling systems, for example. It is intuitive and logical to assume that larger aircraft requires more complex landing gears that have more complex geometric features, which in turn generate more high-frequency noise. Thus, it seems reasonable to correlate the complexity factor in noise prediction to the aircraft takeoff gross weight, which is an easily obtainable parameter in aircraft specifications. To illustrate, a list is given in Table 5 for some of the Boeing family airplanes. It should be pointed out that these are typical values for the aircraft types listed in this table. Within each aircraft type, there are usually various derivative airplanes with different maximum gross takeoff weight. The values listed here should only be used as a reference.

By considering all the discussions above, we define the complexity factor as an increasing function of the number of wheels in the gear, the total length of the main struts and the takeoff gross weight of the aircraft. It is also assumed to account for the effects of wheel track alignment. Thus, we define the complexity factor by the empirical model

$$\eta = \begin{cases} \eta_0 & \text{for main gears,} \\ 0.4\eta_0 & \text{for nose gears,} \end{cases} \tag{42}$$

where η_0 is defined by

$$\eta_0 = 1 + 0.15\left(\frac{W}{W_0}\frac{L}{L_0}\frac{N}{N_0} - 1\right). \tag{43}$$

Here, N and L have been previously defined, respectively, as the number of wheels and the total length of the main struts. We have used W to denote the maximum takeoff gross weight of the aircraft. The subscript "0" in

Table 6
Reference values used in the complexity factor

	W_0 (N)	L_0 (N)	N_0 (m)
Unit	Pounds	Inches	None
Value	150,000 (7.62)	300 (7.62)	72,330 (7.62)

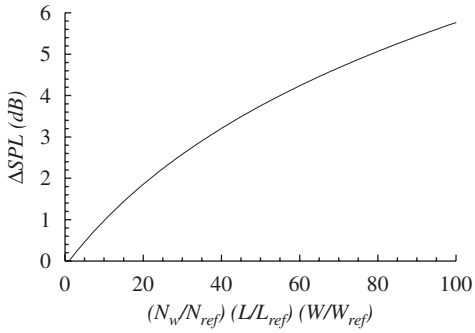

Fig. 8. Increment of landing gear high-frequency noise due to gear complexity.

Eq. (43) indicates reference quantities that are introduced to normalize various quantities. The reference values are defined in Table 6, which are chosen such that the complexity factor η is approximately equal to unity for the Boeing 737 main landing gear. Since the reference values for the takeoff weight and the total strut length are given, respectively, in pounds and inches, the quantities W and L in Eq. (43) should also be specified in these two respective units. It can be noted that though the complexity factor is defined to have the same functional form for both the nose and the main gears, the two cases have different proportionality constants. This is due to the fact that nose gears have fewer components, simpler design and smaller sizes, all leading to less noise generations, as discussed in detail in Ref. [27].

From the empirical formula equation (43), the variations of the far-field high-frequency noise due to the complexity factor plotted in Fig. 8, as the increment in noise as a function of the combined effect of complexity features associated with the wheels, the struts. The model for the geometric complexity groups together the brake systems, the attachments to the struts and other small features, respectively, represented by the number of wheels, the total length of the struts and the gross takeoff weight. The model essentially assigns equal weighting to the three elements that affect the complexity factor. Though more elaborate models can be developed by correlating with test data from various landing gears, which are not currently available, we think the simple model given here should be sufficient for practical applications.

7. Validation

In this section, we apply the empirical models developed in the previous sections to an isolated Boeing 737 main landing gear. The test data for the isolated Boeing 737 main landing gear was obtained in the Boeing Low Speed Acoustic Facility, where a full configuration gear was tested at various flow conditions. The test and the data analysis have been previously published [5,6,16]. The landing gear data were measured by an array of microphones along a straight line in the simulated fly-over plane at various emission angles. The distance between the center of the gear and the microphone at 90° of emission angle is 10 ft. To apply the empirical models for the noise prediction, the dimensions of the main struts need to be supplied as input. For the Boeing 737 main landing gear, the total length of the main struts is found to be 317 in (8.0518 m) and the length scale for the mid-frequency noise component is 4.65 in (0.11811 m). The latter also gives the length scale for the high-frequency component as 0.7 in (0.01778 m), being 15% of the mid-frequency length scale.

The predicted noise from an isolated Boeing 737 main landing gear is plotted in Fig. 9, together with measured data. The plots are for the SPL at three emission angles, as a function of frequency, for four flow Mach numbers. The distance from the gear center to the 90° microphone is 10 ft (3.048 m) and that for the other two microphones is about 11.5 ft (3.505 m). The data shown in this figure are as measured and the predictions include the effects of atmospheric absorption, though those effects are small because of the small distances between the gear and the microphones. The test facility has a low-frequency cutoff about 200 Hz so that no data below this frequency is shown in the figure. Since this is an isolated gear, the directivity factor $D_0(\theta)$ due to the installation effects is set to unity in the predictions. Also, because the data were from a wind tunnel test where the gear and the microphones are both fixed, there is no relative motion between the two and thus no effects due to convective amplification. For meaningful comparison, the predictions are done with the convective amplification removed. The comparisons between predictions and data show good agreement, which is expected since some of the empirical constants in the prediction models are calibrated by the data shown in this figure. It can be seen that there are consistent discrepancies of about a few dB between predictions and data in the frequency range of 800–1000 Hz. This is because the data are dominated by a tone caused by vortex shedding from a torque link, as analyzed in detail in Refs. [7,16]. This particular vortex tone is believed to be specific to this test and has not been observed in other measurements.

To illustrate the contributions from the three spectral components in the landing gear noise, Fig. 10 plots the contributions from the three frequency domains, together with the total noise, for the Boeing 737 main gear at the overhead location with $M = 0.2$. In this case, the three components have comparable amplitudes, leading to a very broadband total noise spectrum. The overall noise levels are compared with data in Fig. 11, for different flow Mach numbers, as a function of the emission angle. Again, the test data are for frequencies above 200 Hz because of the low-frequency cutoff of the test facility. To make the comparison meaningful, the predicted overall sound pressure level is also computed for frequencies above 200 Hz. The overall agreements between predictions and data shown in Figs. 9 and 11 are satisfactory, but there are some discrepancies

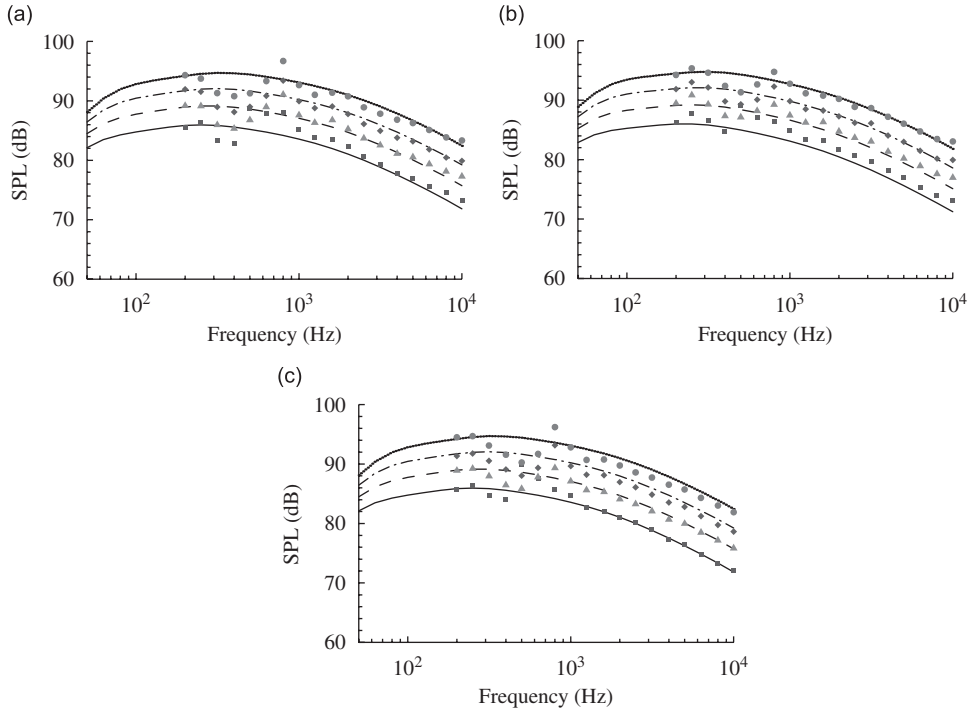

Fig. 9. Comparison of sound pressure levels between predictions and test data for an isolated Boeing 737 main landing gear: (a) for an emission angle of 60°, (b) for 90°, and (c) for 120°. The curves are the predictions and the symbols represent experimental data, with the solid curve and the squares for $M = 0.18$, the dashed curve and the triangles for $M = 0.2$, the dash–dot curve and the diamonds for $M = 0.22$ and the dotted curve and the circles for $M = 0.24$.

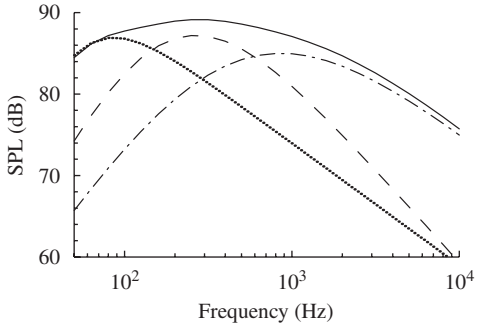

Fig. 10. Spectral decomposition of total noise for the Boeing 737 main landing gear. The solid curve is the total noise and the dotted, the dashed and the dot–dashed curves, respectively, represent the low-, mid- and high-frequency component.

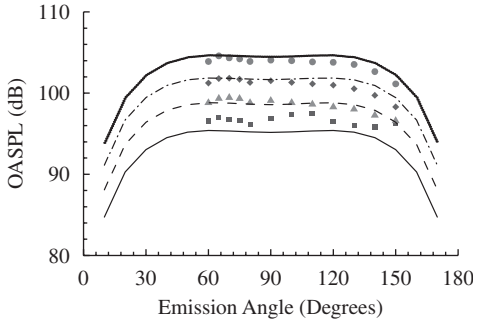

Fig. 11. Comparison of overall sound pressure level between predictions and test data for an isolated Boeing 737 main landing gear. The curves are the predictions and the symbols represent experimental data, with the solid curve and the squares for $M = 0.18$, the dashed curve and the triangles for $M = 0.2$, the dash–dot curve and the diamonds for $M = 0.22$ and the dotted curve and the circles for $M = 0.24$.

between the two, noticeably for the case of lowest Mach number of 0.18. This is due to the fact that the high-frequency noise data scale on the seventh power in Mach number better than the sixth power. This is discussed in Ref. [6] and is attributed to the significant contributions to the landing gear noise from the wake flow. This mechanism is not modeled here, as is clear in the development given in the previous sections, where the noise is scaled on the sixth power in Mach number. This approach is followed here because the difference is small enough to be acceptable for empirical predictions. The variations in the Mach number scaling in the test data are also the reason the results in Fig. 9 are plotted for individual Mach numbers.

To apply the empirical models to the total aircraft landing gear noise, the contributions from the main gears and the nose gear need to be predicted independently and be added incoherently. Furthermore, the installation effects on the mean flow just ahead of the gear also need to be considered. This is because the local flow Mach number under the wing/fuselage can be different from the flight Mach number. From Refs. [8,15], it is noted that for the main landing gear, the lifting effects of the wing typically reduce the local flow velocity to about 70–80% of the flight velocity. This reduced local flow velocity may not apply to the nose gear that is under the fuselage. It is also possible that the local velocity may be even higher than the flight velocity because of the flow acceleration due to the nose geometry of the fuselage. These flow features have been confirmed and quantified in a recent systematic study on local flows at the landing gear locations, which are shown to have significant effects on landing gear noise [27,28].

8. Conclusions and discussions

In this paper, we have presented a component-based model for aircraft landing gear noise prediction. The method starts with the theory of aerodynamic sound generation by moving bodies, which leads to scaling laws governing the functional dependencies of the far-field noise from landing gears on aircraft operational

parameters and landing gear geometric specifications. The total landing gear noise is decomposed into three spectral components, respectively, for the low-, the mid- and the high-frequency domain. The source mechanisms of these three components are, respectively, characterized by three groups of landing gear parts, namely, the wheels, the main struts and the small details of the gear assembly. Empirical modeling and correlation with test data are used to model the spectral properties and the far-field noise directivity in the three frequency domains. The component modeling and prediction have been validated and calibrated by experimental data. An example has been given for the noise of the Boeing 737 aircraft main landing gear, showing good agreements both in parametric trends and in absolute noise levels.

Owing to the complexity of landing gear noise prediction, it is no surprise that there remain unresolved issues in the prediction scheme reported here. One such issue is the installation effects for landing gears installed on aircraft in flight. The aircraft wing and fuselage can significantly change the flow field at the landing gear locations, in comparison with isolated gears in wind tunnel tests, which in turn can significantly change the noise from the gears. The aircraft body can also affect the noise propagation, by reflection and diffraction, potentially leading to different directivity from isolated gears. Both of these are important aspects of landing gear noise generation and propagation, and have been continuously researched on (e.g. Refs. [27,28]).

Another issue related to the installation effects is the potential interactions between the wake flow of the gear and sharp edges of the aircraft wing or the trailing edge of the gear door. This kind of flow interactions would lead to Mach number scaling laws of fifth power. While this has been observed in some aircraft airframe noise measurements, it is by no means conclusive that the wake–edge interaction contributes significantly to the total gear noise. Future research is obviously needed to quantify this contribution, and if proven non-negligible, should be added to the prediction scheme.

Acknowledgments

The work reported here was conducted under NASA Contract NAS1-00086, under the Quiet Aircraft Technology (QAT) program. The author would like to thank the task monitors, Robert A. Golub and Casey Burley, of NASA LaRC, for their support and encouragement. The author would also like to thank Rob Stoker and Ronen Elkoby of the Boeing Company for their assistance in obtaining the test data and gear geometry, and for many helpful discussions on landing gear noise.

References

[1] M.R. Fink, Noise component method for airframe noise, *Journal of Aircraft* 16 (10) (1979) 659–665.
[2] D.G. Crighton, Airframe noise, *Aeroacoustics of Flight Vehicles: Theory and Practice*, NASA RP-1258, Vol. 1, 1991, pp. 391–447.
[3] M.G. Smith, L.C. Chow, Prediction method for aerodynamic noise from aircraft landing gear, *AIAA Paper 98-2228*, June 1998.
[4] M.G. Smith, L.C. Chow, Validation of a prediction model for aerodynamic noise from aircraft landing gear, *AIAA Paper 2002-2581*, June 2002.
[5] R. Sen, B. Hardy, K.J. Yamamoto, Y.P. Guo, G. Miller, Airframe noise sub-component definition and model, NASA Informal Contract Report, NAS1-97040, 2000.
[6] Y.P. Guo, K.J. Yamamoto, R.W. Stoker, An experimental study on aircraft landing gear noise, *Journal of Aircraft* 43 (2) (2006) 306–317.
[7] L. Lopes, K. Brentner, P. Morris, G. Lilley, D. Lockhard, Complex lending gear noise prediction using a simple toolkit, *AIAA Paper 2005-1202*, Reno, Nevada, January 2005.
[8] Y.P. Guo, A semi-empirical model for aircraft landing gear noise prediction, *AIAA Paper 2006-2627*, Cambridge, MA, May 2006.
[9] Y.P. Guo, A statistical model for landing gear noise prediction, *Journal of Sound and Vibration* 282 (2005) 61–87.
[10] J.E. Ffowcs Williams, D.L. Hawkings, Sound generation by turbulence and surfaces in arbitrary motion, *Philosophical Transactions of Royal Society of London A* 264 (1969) 321.
[11] D.G. Crighton, Basic principles of aerodynamic noise generation, *Progress in Aerospace Sciences* 16 (1) (1975) 31–96.
[12] M.J. Lighthill, On sound generated aerodynamically I. General theory, *Proceedings of the Royal Society of London A* 211 (1952) 564–587.
[13] D.G. Crighton, A.P. Dowling, J.E. Ffowcs Williams, M. Hekle, F.G. Leppington, *Modern Methods in Analytical Acoustics*, Springer, New York, 1992.
[14] H. Heller, W. Dobrzynski, Sound radiation from aircraft wheel-well/landing-gear configuration, *Journal of Aircraft* 14 (8) (1977) 768–774.

[15] W. Dobrzynski, H. Buchholz, Full-scale noise testing on Airbus landing gears in the German Dutch Wind Tunnel, *AIAA Paper 97-1597*, May 1997.
[16] R.W. Stoker, Landing Gear Noise Test Report, NASA Contract NAS1-97040, 1997.
[17] U. Michel, W. Qiao, Directivity of landing-gear noise based on flyover measurements, *AIAA Paper 99-1956*, May 1999.
[18] W. Dobrynski, L.C. Chow, P. Guion, D. Shiells, Research into landing gear airframe noise reduction, *AIAA Paper 2002-2409*, June 2002.
[19] S.M. Jaeger, N.J. Burnside, P.T. Soderman, W.C. Horne, K.D. James, Microphone array assessment of an isolated 26%-scale high fidelity landing gear, *AIAA Paper 2002-2410*, June 2002.
[20] W.C. Horne, K.D. James, B.L. Storms, Flow survey of the wake of a commercial transport main landing gear, *AIAA Paper 2002-2407*, June 2002.
[21] L.C. Chow, K. Mau, H. Remy, Landing gear and high lift devices airframe noise research, *AIAA Paper 2002-2408*, June 2002.
[22] L.S. Hedges, A. Travin, P.R. Spalart, Detached-eddy simulations over a simplified landing gear, *Journal of Fluids Engineering* 124 (2) (2002) 413–423.
[23] F. Li, M.R. Khorrami, M.R. Malik, Unsteady simulation of a landing gear flow field, *AIAA Paper 2002-2411*, June 2002.
[24] F.J. Souliez, L.N. Long, P.J. Morris, A. Sharma, Landing gear aerodynamic noise prediction using unstructured grids, *AIAA Paper 2002-0799*, June 2002.
[25] D. Lockard, M. Khorrami, Aeroacoustic analysis of a simplified landing gear, *AIAA Paper 2003-3111*, Hilton Head, SC, May 2003.
[26] D. Lockard, M. Khorrami, High resolution calculation of a simplified landing gear, *AIAA Paper 2004-2887*, Manchester, UK, 2004.
[27] Y.P. Guo, An improved landing gear noise prediction scheme, NASA Contract Report NAS1-NNL04AA11B Task NNL06AB63T, November 2006.
[28] Y.P. Guo, A study on local flow variations for landing gear noise research, NASA Contract Report NAS1-NNL04AA11B Task NNL06AB63T, November 2006.